Carbon 101 (2016) 107–113

Contents lists available at ScienceDirect

Carbon

journal homepage: www.elsevier.com/locate/carbon

Ultra-low thermal conductivity in graphene nanomesh

Tianli Feng, Xiulin Ruan*

School of Mechanical Engineering and the Birck Nanotechnology Center, Purdue University, West Lafayette, IN 47907-2088, USA

ARTICLE INFO

Article history:
Received 2 December 2015
Received in revised form
15 January 2016
Accepted 22 January 2016
Available online 26 January 2016

ABSTRACT

Graphene nanomesh (GNM), a new nanostructure of graphene, has attracted extensive interest recently due to the promising chemical, electronic and photonic applications. In this paper, another important property – thermal conductivity is systematically investigated by using molecular dynamics simulations. The thermal conductivity (κ) is found to be extremely low, up to more than 3 orders lower than the pristine single layer graphene. Roughly, κ decreases exponentially with increasing porosity and linearly with decreasing neck width, and is not temperature sensitive in the range of 300 K–700 K. κ of GNMs is found to be even up to 200-fold lower than the graphene nanoribbons (GNR), a potential thermoelectric material, of the same neck width and boundary-to-area ratio. The extremely low κ in the GNM makes it a potential candidate for thermoelectrics. The phonon participation spectra show that the low κ in GNM is due to the localization and phonon back scattering around the nanopores. We also find that the phonon coherence in two dimensional superlattice GNM indeed exists, but is not as important as in the one dimensional superlattices. The isotope effect is negligible. The thermal conductivity reduction by edge passivation increases with increasing neck width and porosity.

1. Introduction

Graphene nanomesh (GNM), a graphene sheet with periodically arranged nanopores, has attracted extensive attention in recent a few years due to the promising applications in the field-effect transistors [1–8], vapor detection [9–11], photothermal therapy [12] and energy storage [13]. GNMs can be viewed as networks of graphene nanoribbons (GNRs), but GNMs have significantly higher on-off ratio and larger supported current than GNRs [1,14]. It has also been shown that GNMs have a strong negative differential conductance which is useful for high frequency applications [15]. Those new electronic and electrical properties are mainly owing to the opening of a tunable band gap by the periodically arranged pores, whereas the new chemical properties are mainly owing to the large porosity.

Although the electronic, chemical and photonic properties of GNMs have been extensively studied [1–13], the thermal properties of GNMs has seldom been investigated [16,17]. Since the GNM based devices work at a certain temperature region, the thermal transport study is important to guide thermal management. Also, the thermal conductivity κ is a key factor to determine the application of GNM to thermoelectric energy conversion [18], since the opening of a band gap in GNM makes it possible for thermoelectrics. The GNMs can be viewed as networks of GNRs, which have been shown to have a high thermoelectric figure of merit ZT [19,20] of 2–3 at room-to-high temperatures by adjusting the dopants and engineering the boundaries.

2. Simulation setup

In this work, we systematically investigate the thermal conductivity in GNMs and discuss potential applications in thermoelectrics. In Fig. 1, we show the GNM samples with (a) squarely arranged circular pores (SC), (b) hexagonally arranged circular pores (HC) and (c) hexagonally arranged hexagonal pores (HH). Previous theoretical work that studied the electronic property covered all three types of structures [14,15,21–25], while experimental work was mainly focused on the HC-GNM [1–8,10,11]. The current experimental technique can fabricate the GNM with neck widths as low as 5 nm [1], and this value should be further reduced as the technique develops. The minimum neck widths of the GNM is about 0.75 nm to maintain the stability of the atomic structure, based on our molecular dynamics (MD) simulations at 300 K. Therefore, in this work, each GNM structure is studied with three different neck widths of 10 nm, 5 nm and 0.75 nm. For each value of the neck width, we investigate the thermal conductivity with a

* Corresponding author.
E-mail address: ruan@purdue.edu (X. Ruan).

http://dx.doi.org/10.1016/j.carbon.2016.01.082
0008-6223/

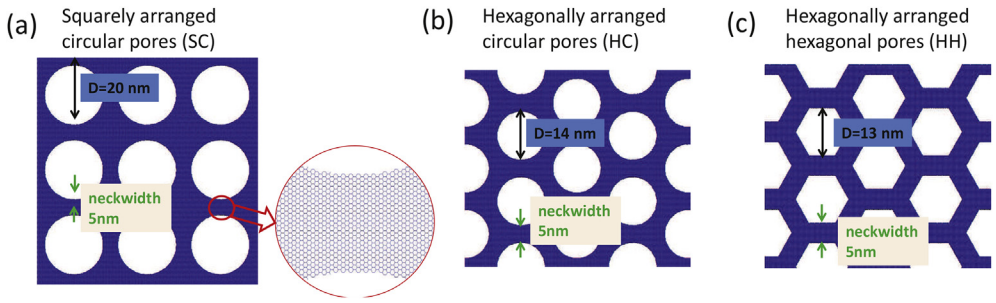

Fig. 1. Illustration of the structures for (a) SC-GNMs, (b) HC-GNMs and (c) HH-GNMs. The samples are of 5 nm neck width and porosity of 0.5. (A color version of this figure can be viewed online).

wide range of porosity P, which is determined by the neck width W_{neck} and the pore diameter D with $P = \frac{\pi}{4}(W_{neck}/D + 1)^{-2}$ in the SC-GNM, $P = \frac{\pi}{2\sqrt{3}}(W_{neck}/D + 1)^{-2}$ in the HC-GNM and $P = (W_{neck}/D + 1)^{-2}$ in the HH-GNM. Limited by the condition of $(W_{neck}/D + 1)^{-2} < 1$, the upper limits of P in those structures are 79%, 91% and 100%, respectively. In this work, we study the SC-GNM, HC-GNM and HH-GNM with porosity varying in 10–75%, 10–85% and 10–99%, respectively, and as a result, the pore diameter varies from 0.3 nm to 200 nm.

The thermal conductivity κ of the GNMs is calculated by the Green–Kubo (GK) method based on equilibrium molecular dynamics (EMD) performed using LAMMPS [26] with the optimized Tersoff potential [27], which produces significantly better lattice properties such as the lattice constant and phonon dispersion relation than the original one [28] in graphene. In the in-plane directions, we use the periodic boundary conditions. The total simulation time and step interval are set as 5 ns and 0.5 fs, respectively. The autocorrelation length is set as 100 ps which is long enough to obtain the converged heat current auto-correlation function (HCACF). Our GK-MD simulation shows that the thermal conductivity κ_0 of the pristine single layer graphene (SLG) at room temperature is converged after the size of the simulation domain increases to 10 nm × 10 nm. The thermal conductivity of SLG given by EMD based on the optimized Tersoff potential is about ~1100 W/mK at the classical room temperature without quantum correction, as also shown in our previous papers [29,30]. Based on the different requirements for eliminating the size effect in different GNM samples, the size of the simulation domain in this work varies from 20 nm × 20 nm–800 nm × 800 nm with the total number of atoms ranging from 30,000 to 3,000,000. All the thermal conductivity values in this work are averaged in the armchair and zigzag directions with three independent simulations.

3. Results and discussions

3.1. Effects of pore size, pore shape, neck width, porosity and temperature

The thermal conductivities κ of the GNMs relative to that of the pristine SLG at room temperature (κ_0) with respect to the neck width and the porosity are summarized in Fig. 2. A porosity of 10% yields a significant reduction in κ by about 80%, 90% and 98.5% in GNMs with the neck width of 10 nm, 5 nm and 0.75 nm, respectively. As shown in Fig. 2(d), HC-GNM has the lowest thermal conductivity for the same neck width and porosity. It can be seen that at high porosity, κ of HC-GNM can be 50% lower than the others. Generally κ/κ_0 reduces exponentially with increasing porosity and linearly with decreasing neck width. The linear dependence on neck width at fixed porosities is shown in Fig. 3. At the porosity of 50%, κ/κ_0 reaches as low as 7%, 4% and 0.4% for the three neck widths, respectively. The GNMs fabricated in the experiment [1,3–7,10] often have a high porosity, which results in extremely low thermal conductivity. For instance, κ reaches about 0.1% and 0.05% of κ_0 in the 85%-porous HC-GNM and the 99%-porous HH-GNM, respectively. The extremely low thermal conductivity in GNMs goes far below the Fourier classic Eucken model [31,32], $\kappa_{porous}/\kappa_0 = (1 - P)/(1 + P/2)$, by 1–2 orders. The Eucken model is only applicable to the structures with size being larger than the phonon mean free path (MFP). In GNMs, where the case is opposite, the neck width of ~10 nm is significantly smaller than the effective phonon MFP of around 240 nm [33] in the pristine SLG. Besides the neck width and the porosity effects, the temperature T dependence of κ/κ_0 in the SC-GNM samples is shown in Fig. 4. In contrast to the rapidly decreasing κ with T in the pristine SLG, κ of GNMs is generally not sensitive to T. Additionally, as the neck width is thin enough, κ of GNMs usually increases with the rise of T, which contributes less to the reduction of phonon relaxation time than to the increase of phonon specific heat.

3.2. Potential thermoelectric property compared to graphene nanoribbon

More interestingly, the thermal conductivity in GNMs is found to be significantly lower than that of GNRs. In Fig. 5, we show the relative thermal conductivity ($\kappa_{GNM}/\kappa_{GNR}$) between GNMs and GNRs with (a) the same (neck) width and (b) the same boundary-to-area ratio at room temperature. The thermal conductivities in the 10%-porous GNMs with neck widths of 10 nm, 5 nm and 0.75 nm are found to be 65%, 75% and 85% lower than κ_{GNR} of the same neck width, respectively. At high porosities, κ_{GNM} can reach 10–200 times lower than GNRs with the same neck width. Sevinçli et al. reduced the thermal conductivity of the 0.75 nm-GNRs by 69% via a sharp zigzag-shape reconstruction. However, the thermal conductivity is still 6-fold and 60-fold higher than the thermal conductivity of the 50%-porous GNM and the 99%-porous HH-GNM [19] of the same neck width, respectively. The thermal conductivity of the sharp zigzag-shape GNR was further reduced by 96.2% via an extra 50%-^{14}C doping [19] with precursor distribution, and has been shown to achieve its highest ZT of 2 at room temperature with a 98.8% thermal conductance reduction compared to the pristine rectangular GNR. For comparison, without any edge engineering or isotope doping, the thermal conductivity of the 99%-porous GNM is 0.5% of that in the pristine rectangular GNR and is 2.4 times lower than the κ of the 50%-^{14}C doped sharp-zigzag-shape GNRs in Ref. [19]. This ultra-low κ illustrates a possibility of a high ZT in GNMs if a similar power factor σS^2 is achieved, which can be calculated via a precise First Principle calculation. On the one hand, the electrical conductivity σ in GNMs has been shown to be comparable to that in rectangular-shape GNRs of the same (neck) width

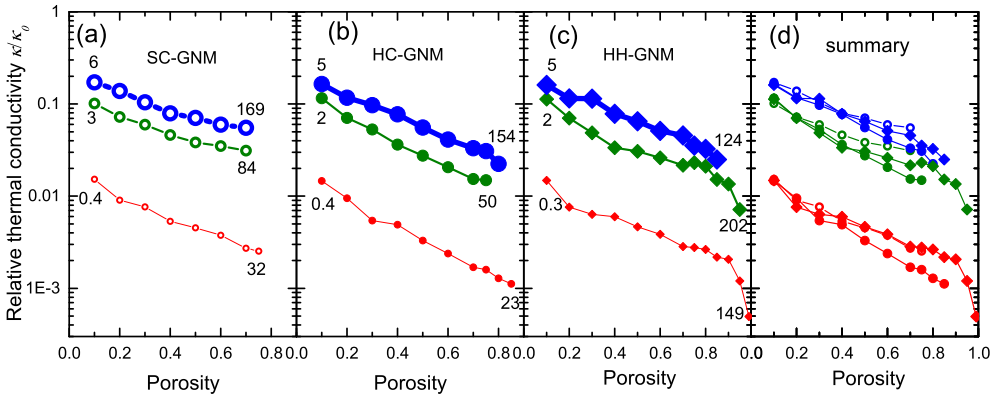

Fig. 2. The relative thermal conductivity κ/κ_0 in (a) the SC-GNMs, (b) the HC-GNMs, and (c) the HH-GNMs as a function of the porosity for three different neck widths: $W_{neck} = 10$ nm (blue), $W_{neck} = 5$ nm (green), and $W_{neck} = 0.75$ nm (red). κ_0 represents the thermal conductivity of the pristine SLG at room temperature. The thicker curves represent thicker neck widths. The numbers at the two ends of each curve indicate the corresponding pore diameters (nm) of the GNM samples. The figure (d) plots a summary for the comparison among the SC, HC, and HH GNMs. (A color version of this figure can be viewed online).

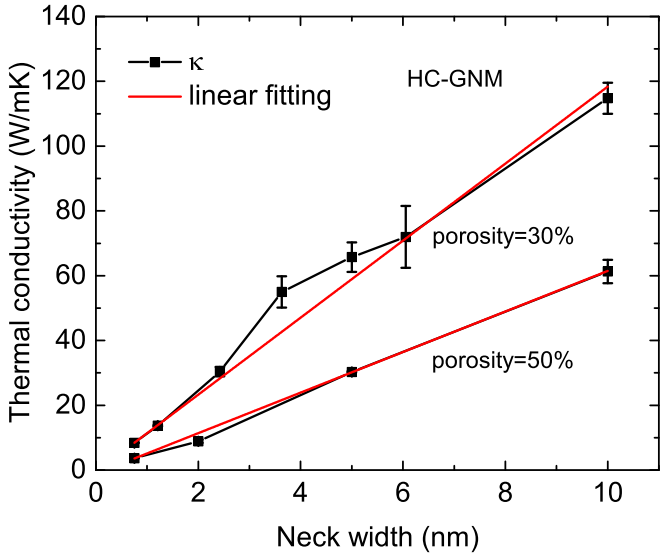

Fig. 3. HC-GNMs with 30% and 50% porosities are chosen to illustrate the linear neck width dependence of thermal conductivity. (A color version of this figure can be viewed online).

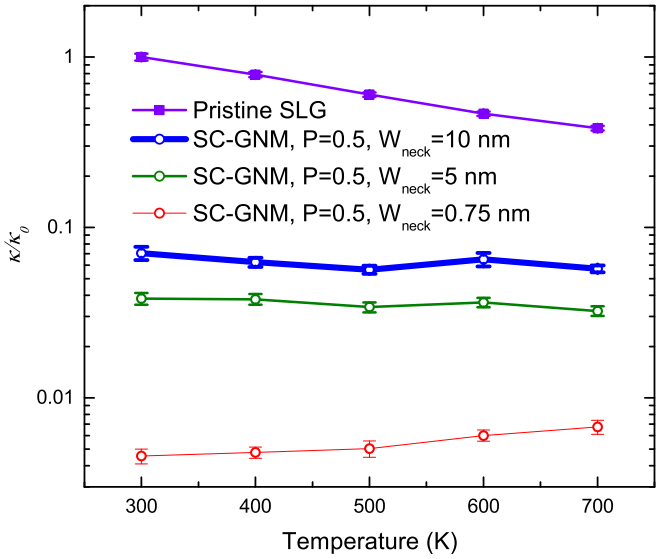

Fig. 4. The relative thermal conductivity κ/κ_0 versus the temperature. (A color version of this figure can be viewed online).

[1,34,35] and thus should be higher than that in sharp zigzag-shape GNRs. On the other hand, the Seebeck coefficient S of GNMs is possibly not low considering its direct band gap and semiconducting behavior. Moreover, S of GNMs may be tuned in the same way as GNRs by adjusting the neck width and using dopants [19,36] since GNMs can be viewed as an interconnected network of GNRs [1]. Compared to the sharp-zigzag-shape GNRs with 50%-^{14}C isotopes of a precursor distribution, which are hard to be fabricated or applied to a real thermoelectric device, the GNMs can be fabricated on a large sheet of graphene and thus be easier for practical applications. The possible enhancement of ZT in GNMs owes to strong scattering of phonons and less scattering of electrons, whose MFP is significantly shorter. Based on this fact, Thiyagarajan et al. achieved a low thermal conductivity of 0.9 W/mK and a high electrical conductivity of 6660 S/m simultaneously in a three-dimensional graphene nanonetwork [37].

3.3. Phonon localization and back scattering

The ultra-low thermal conductivity in GNMs is interpreted by studying phonon localization using a vibrational eigen-mode analysis. The phonon participation ratio, defined as

$$\xi_\lambda = \frac{1}{N\sum_{i=1}^{N}\left(\sum_{\alpha=1}^{3} e_{i\alpha,\lambda}^{*} e_{i\alpha,\lambda}\right)^2}, \quad (1)$$

describes the fraction of atoms participating in a particular vibration mode λ. $e_{i\alpha,\lambda}$ is the ith component of the eigenvector of the mode λ in the α-direction, with α representing x, y and z. N is the total number of atoms. The participation ratio varies from 0 for a complete-localized state to 1 for a complete-non-localized state. In Fig. 6, we compare the participation ratio spectra in the pristine SLG, GNRs and GNMs. The high ξ_λ value of 1 in the pristine SLG demonstrates the global vibrations with all atoms participating in, which explains its extremely high thermal conductivity. After cutting off the two edges and the periodic pores, the ξ_λ in GNRs and GNMs is reduced to about 0.7 and 0.5, respectively. The phonon participation ratio elucidates the phonon localization as one possible cause of the ultra-low thermal conductivity in GNMs. Nevertheless, ξ_λ is still large in the low-frequency region, indicating

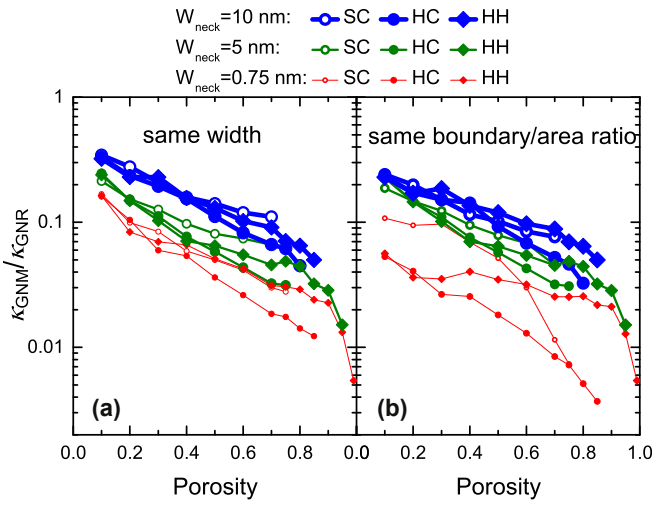

Fig. 5. The thermal conductivity ratio $\kappa_{GNM}/\kappa_{GNR}$ between GNRs and GNMs with (a) the same neck width and (b) the same boundary-to-area ratio at 300 K. The thicker curves represent the GNMs with the thicker neck widths. (A color version of this figure can be viewed online).

distribution defined by Ref. [38] $E_i = \sum_{\lambda}\sum_{\lambda}(n+1/2)\hbar\omega e^*_{i\alpha,\lambda}e_{i\alpha,\lambda}\delta(\omega-\omega_\lambda)$, with higher energy representing higher localization and lower energy representing higher transmission, as shown in Fig. 7.

Besides the phonon localization analysis, a model of calculating the thermal conductivity in GNMs is studied. For simplicity, we drop the mode dependence of phonon MFP Λ and employ the effective MFP with the Matthienssen's rule being applied, $\Lambda^{-1} = \Lambda_0^{-1} + \Lambda_b^{-1}$ and $\kappa^{-1} = \kappa_0^{-1} + \kappa_b^{-1}$. Λ_0 is the effective MFP in pristine SLG with the value of 240 nm [33]. $\Lambda_b = (1+p)/(1-p)w$ is the MFP for a phonon to hit the boundary, where p is the specularity parameter ranging from 0 for completely rough edges to 1 for completely smooth edges. In summary, the thermal conductivity of GNRs and GNMs are given by

$$\kappa_{GNR} = \kappa_0 \frac{1}{1+\Lambda_0/\Lambda_b}, \Lambda_b = \frac{1+p_r}{1-p_r}w, \tag{2}$$

and

$$\kappa_{GNM} = \kappa_0 \frac{1}{1+\Lambda_0/\Lambda_b}(1-P), \Lambda_b = \frac{1+p_m}{1-p_m}\overline{w}, \tag{3}$$

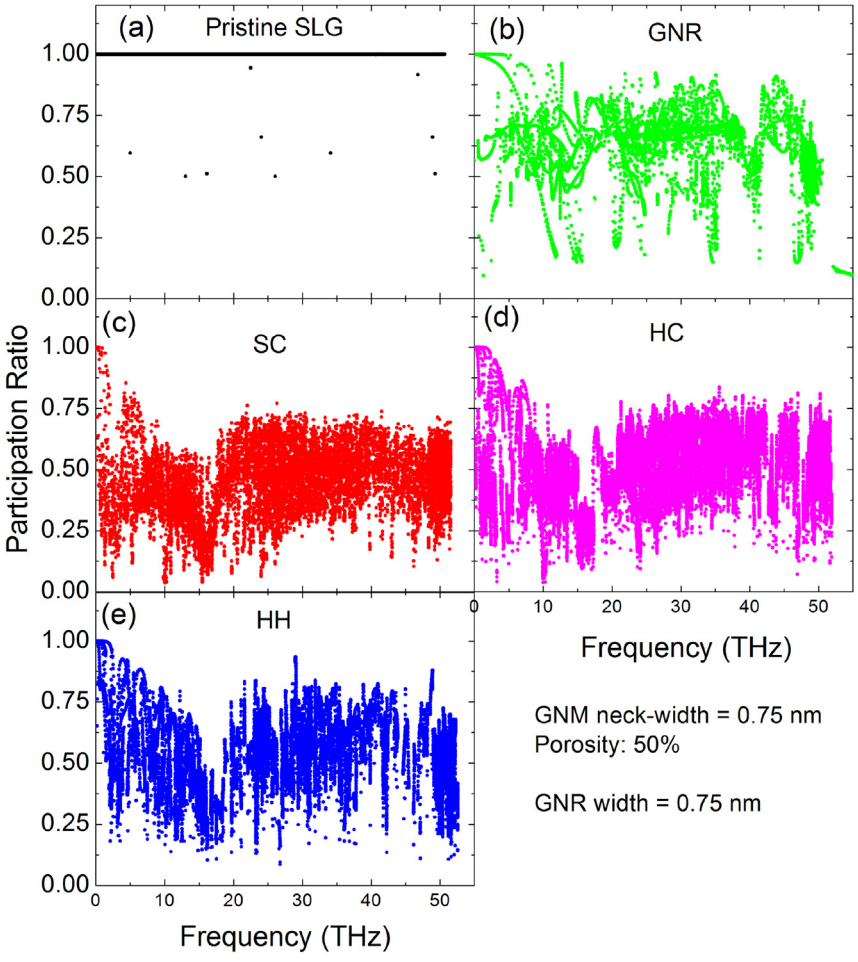

Fig. 6. The phonon participation ratio spectra at 300 K for (a) the pristine SLG, (b) the GNR, (c) the SC-GNM, (d) the HC-GNM, and (e) the HH-GNM samples. The GNR and GNMs are of the same neck width of 0.75 nm and the GNMs have a porosity of 50%. (A color version of this figure can be viewed online).

that the long-wavelength phonons remain non-localized in GNRs and GNMs. The phonon localization is illustrated by the energy

respectively. In Eq. (3), the factor $1-P$ represents the loss of material based on the effective medium approximations [39].

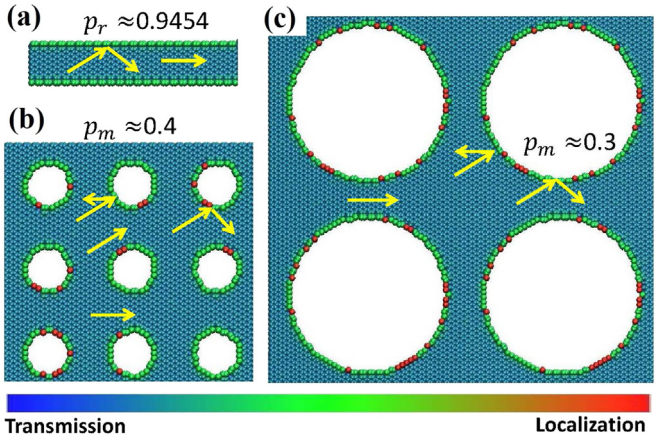

Fig. 7. The normalized energy distribution in (a) the GNR, (b) the 20%-porous GNM and (c) the 50%-porous GNM with the same neck width of 2 nm. The phonon transport and the back scattering are sketched. (A color version of this figure can be viewed online).

$\kappa_0 1/1 + \Lambda_0/\Lambda_b$ represents the lattice thermal conductivity of the imagined fully dense graphene materials with the boundaries the same as the GNMs. The equivalent width of GNM $\overline{w} = D/2(1/P - 1)$, deviating little from W_{neck}, is the width of the equivalent GNR that owns the same boundary-to-area ratio with the GNM. p_r and p_m represent the specularity parameters in GNRs and GNMs respectively. p_r changes little with the width varying from 0.75 nm to 20 nm. p_m is calculated for each particular GNM by Eq. (3). It is noted that the p_m is an effective specularity parameter that not only accounts for the smoothness of the boundaries but also includes the factor of phonon localization and back scattering by the boundaries (Fig. 7(b) and (c)). As shown in Fig. 8, the GNRs own a high specularity of about 0.95 which agree with Ref. [40]. In contrast, due to the phonon back scattering by the nanopores in GNMS, p_m is typically around 0.2–0.5 and decreases as the porosity P increases in SC-GNMs and HC-GNMs. Interestingly, p_m is

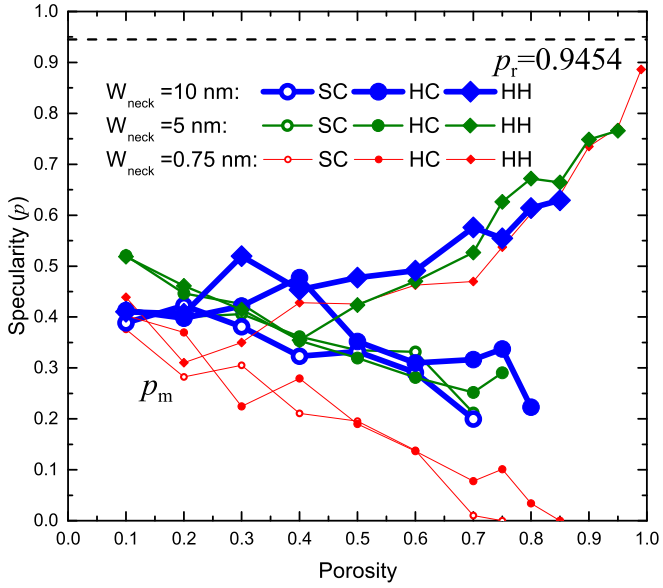

Fig. 8. The specularity parameters, p_r and p_m, of GNRs and GNMs calculated from Eqs. (2) and (3), respectively, at room temperature. p_r is fitted from the GNRs with the width varying from 0.75 nm to 20 nm. (A color version of this figure can be viewed online).

approaching to the GNR limit in HH-GNMs as P increases. This is consistent to the fact that SC-GNMs and HC-GNMs approach the interconnected network of GNRs with curved edges, while HH-GNM approaches those with straight edges.

3.4. Phonon coherence in two dimensional superlattice

GNMs can also be viewed as two dimensional superlattices constructed by the periodic pores, in which the phonon coherence is of great interest. As a comparison, it is well known that the phonon coherent in one dimensional superlattice is important, e.g., Wang et al. [41] have shown that the random multilayer structures have much lower thermal conductivities than superlattice due to the break of phonon coherence. However, in two dimensional superlattice, periodic boron nitride islands doped graphene, the break of periodicity of BN islands does not make much difference to the thermal conductivity. Such phenomenon is understandable by comparing the freedoms of the phonon transport. In 1D superlattices, the phonon transport is confined in one specific direction and thus the phonon coherence can be easily broken by breaking the periodicity. In contrast, in 2D or 3D superlattices phonons are harder to be blocked by breaking the periodicity since they can transport energy in a higher degree of freedom. Here, to probe the phonon coherence in the 2D superlattice GNM, we investigate the effect of random pore distribution on the thermal conductivity. Take the 30%-porous GNMs as examples, we find that the thermal conductivity of GNMs is reduced by 20–40% when the order of pores is broken. This result indicates that the phonon coherence in GNM still exists but is not as important as in 1D superlattices.

3.5. Effect of isotope and edge passivation

Isotopes and edge passivation are commonly seen in real GNM devices [42]. Isotopes induce mass disorder and phonon-isotope scattering and thus reduce the thermal conductivity [43]. We compare the thermal conductivities in the intrinsic ^{12}C-GNMs, intrinsic ^{13}C-GNMs, and randomly 50%-^{13}C doped GNMs (Fig. 9(b)). We find that the random 50% ^{13}C doping makes negligible difference to the thermal conductivity of the intrinsic ^{12}C-GNM or the intrinsic ^{13}C-GNM, in contrary to that in the pristine SLG [30,44,45] and other pristine materials [43,46] in which isotopes remarkably reduce the thermal conductivity. This is because in the pristine materials, the phonon isotope scattering induced by the isotope mass disorder is comparable to the intrinsic phonon anharmonic scattering and thus makes a huge difference to the total phonon transport. Whereas in GNMs, the large phonon localization induced by boundary scattering overwhelms the mass disorder induced by isotopes, and as a result, the phonon transport is scarcely affected by isotope doping. Also, we find that the thermal conductivity is slightly reduced by edge passivation (Fig. 9(c)) at small neck widths, in contrast the large reduction in GNRs [47], by using the Brenner potential [48] to model the interaction between hydrogen atoms and the edge carbon atoms. The effect of passivation increases with increasing neck width and porosity. Among the simulations we conducted, the largest reduction by H passivation can reach as high as 50% for the neck width of 7 nm.

4. Conclusions

To conclude, the thermal conductivity of GNMs is studied systematically by using Green–Kubo molecular dynamics spreading a wide scale from nm to μm with different neck widths, pore shapes, pore arrangements, and temperatures. The GNMs are found to have an extremely low thermal conductivity, which is significantly lower than that in the GNRs with the same width and boundary-to-area

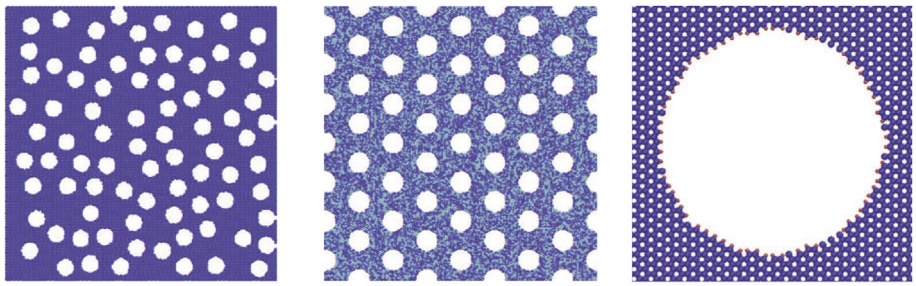

Fig. 9. (a) Random pore distributed graphene. (b) The GNM with 50% ^{13}C isotopes. (c) The GNM with edge passivation by hydrogenation. (A color version of this figure can be viewed online).

ratio. A rough analysis indicates the possibility of a considerably high ZT in GNMs. Given that GNMs can be fabricated in large sheets of graphene, which is easier for the practical application than the nano-size GNRs [1], the GNM devices may become a better thermoelectric candidate than GNRs. The ultra-low thermal conductivity in GNMs arises from the large phonon localization and the back phonon scattering around the nanopores. An effective specularity parameter is found to be around 0.2–0.5 in GNMs, which is much lower than the 0.95 in GNRs. Also, we find that the thermal conductivity of GNMs is reduced by 20–40% when the order of pores is broken, indicating the existence as well as less importance of phonon coherence in two-dimensional superlattices compared to one-dimensional superlattices. We have found that the isotope effect is negligible. The κ reduction by edge passivation is small compared to GNR, but increases as the neck width or porosity increases.

Acknowledgments

We would like to thank Kelly Rickey for the proof reading and Yan Wang for the helpful discussions. Simulations were performed at the Rosen Center for Advanced Computing (RCAC) of Purdue University. The work was partially supported by the National Science Foundation (Award No. 1150948).

References

[1] J. Bai, X. Zhong, S. Jiang, Y. Huang, X. Duan, Nat. Nanotechnol. 5 (2010) 190. ISSN 1748-3395, http://www.pubmedcentral.nih.gov/articlerender.fcgi?artid=2901100&tool=pmcentrez&rendertype=abstract.
[2] I. Jung, H.Y. Jang, J. Moon, S. Park, Nanoscale 6 (2014) 6482. ISSN 2040-3372, http://www.ncbi.nlm.nih.gov/pubmed/24837501.
[3] A. Sinitskii, J.M. Tour, J. Am. Chem. Soc. 132 (2010) 14730. ISSN 1520-5126, http://www.ncbi.nlm.nih.gov/pubmed/20886879.
[4] X. Liang, Y.-S. Jung, S. Wu, A. Ismach, D.L. Olynick, S. Cabrini, J. Bokor, Nano Lett. 10 (2010) 2454. ISSN 1530-6992, http://www.ncbi.nlm.nih.gov/pubmed/20540552.
[5] G. Ning, Z. Fan, G. Wang, J. Gao, W. Qian, F. Wei, Chem. Commun. (Cambridge, England) 47 (2011) 5976. ISSN 1364-548X, http://www.ncbi.nlm.nih.gov/pubmed/21475753.
[6] Z. Zeng, X. Huang, Z. Yin, H. Li, Y. Chen, H. Li, Q. Zhang, J. Ma, F. Boey, H. Zhang, Adv. Mater. (Deerfield Beach, Fla.) 24 (2012) 4138. ISSN 1521-4095, http://www.ncbi.nlm.nih.gov/pubmed/22434606.
[7] M. Wang, L. Fu, L. Gan, C. Zhang, M. Rümmeli, A. Bachmatiuk, K. Huang, Y. Fang, Z. Liu, Sci. Rep. 3 (2013) 1238. ISSN 2045-2322, http://www.nature.com/doifinder/10.1038/srep01238.
[8] D.P. Yang, X. Wang, X. Guo, X. Zhi, K. Wang, C. Li, G. Huang, G. Shen, Y. Mei, D. Cui, J. Phys. Chem. C 118 (2014) 725. http://pubs.acs.org/doi/abs/10.1021/jp409898d.
[9] A. Esfandiar, N. Kybert, E.N. Dattoli, Appl. Phys. Lett. 103 (2013) 183110. http://scitation.aip.org/content/aip/journal/apl/103/18/10.1063/1.4827811.
[10] R.K. Paul, S. Badhulika, N.M. Saucedo, A. Mulchandani, Anal. Chem. 84 (2012) 8171. ISSN 1520-6882, http://www.ncbi.nlm.nih.gov/pubmed/22931286.
[11] J. Liu, H. Cai, X. Yu, K. Zhang, X. Li, J. Li, N. Pan, Q. Shi, Y. Luo, X. Wang, J. Phys. Chem. C 116 (2012) 15741. ISSN 1932-7447, http://pubs.acs.org/doi/abs/10.1021/jp303265d.
[12] O. Akhavan, E. Ghaderi, Small (Weinheim an der Bergstrasse, Germany) 9 (2013) 3593. ISSN 1613-6829, http://www.ncbi.nlm.nih.gov/pubmed/23625739.
[13] L. Jiang, Z. Fan, Nanoscale 6 (2014) 1922. ISSN 2040-3372, http://www.ncbi.nlm.nih.gov/pubmed/24301688.
[14] S. Berrada, V.H. Nguyen, Appl. Phys. Lett. 103 (2013) 183509. http://scitation.aip.org/content/aip/journal/apl/103/18/10.1063/1.4828496.
[15] V.H. Nguyen, F. Mazzamuto, J. Saint-Martin, A. Bournel, P. Dollfus, Nanotechnology 23 (2012) 065201. ISSN 0957–4484, http://stacks.iop.org/0957-4484/23/i=28/a=289502?key=crossref.14d1dd76173b651267ee787f11584de3.
[16] B.-Y. Cao, W.-J. Yao, Z.-Q. Ye, Carbon 96 (2016) 711. ISSN 0008-6223, http://www.sciencedirect.com/science/article/pii/S0008622315303158.
[17] L. Hu, D. Maroudas, J. Appl. Phys. 116 (2014) 184304. ISSN 0021-8979, http://scitation.aip.org/content/aip/journal/jap/116/18/10.1063/1.4901335.
[18] Y. Xu, Z. Li, W. Duan, Small 10 (2014a) 2182. ISSN 1613-6829, http://dx.doi.org/10.1002/smll.201303701.
[19] H. Sevinçli, C. Sevik, T. Çagin, G. Cuniberti, Sci. Rep. 3 (2013) 1228. ISSN 2045-2322, http://www.pubmedcentral.nih.gov/articlerender.fcgi?artid=3565174&tool=pmcentrez&rendertype=abstract.
[20] H. Sevinçli, G. Cuniberti, Phys. Rev. B 81 (2010) 113401. ISSN 1098-0121, http://link.aps.org/doi/10.1103/PhysRevB.81.113401.
[21] W. Oswald, Z. Wu, Phys. Rev. B 85 (2012) 115431. ISSN 1098-0121, http://link.aps.org/doi/10.1103/PhysRevB.85.115431.
[22] N.C.B. Mostério, A.F. Fonseca, Phys. Rev. B 89 (2014) 195437. ISSN 1098-0121, http://link.aps.org/doi/10.1103/PhysRevB.89.195437.
[23] H. Sahin, S. Ciraci, Phys. Rev. B 84 (2011) 035452. ISSN 1098–0121, http://link.aps.org/doi/10.1103/PhysRevB.84.035452.
[24] H.-X. Yang, M. Chshiev, D.W. Boukhvalov, X. Waintal, S. Roche, Phys. Rev. B 84 (2011) 214404. ISSN 1098-0121, http://link.aps.org/doi/10.1103/PhysRevB.84.214404.
[25] K. Lopata, R. Thorpe, S. Pistinner, X. Duan, D. Neuhauser, Chem. Phys. Lett. 498 (2010) 334. ISSN 00092614, http://linkinghub.elsevier.com/retrieve/pii/S0009261410011929.
[26] S. Plimpton, J. Comput. Phys. 117 (1995) 1. ISSN 0021-9991, http://www.sciencedirect.com/science/article/pii/S002199918571039X.
[27] L. Lindsay, D.A. Broido, Phys. Rev. B 81 (2010) 205441. ISSN 1098-0121, http://link.aps.org/doi/10.1103/PhysRevB.81.205441.
[28] J. Tersoff, Phys. Rev. B 39 (1989) 5566. http://link.aps.org/doi/10.1103/PhysRevB.39.5566.
[29] B. Qiu, X. Ruan, arXiv preprint arXiv:1111.4613 (2011) arXiv:1111.4613v1, http://arxiv.org/abs/1111.4613v1.
[30] T. Feng, X. Ruan, Z. Ye, B. Cao, Phys. Rev. B 91 (2015) 224301. http://link.aps.org/doi/10.1103/PhysRevB.91.224301.
[31] J. Tang, H.-T. Wang, D.H. Lee, M. Fardy, Z. Huo, T.P. Russell, P. Yang, Nano Lett. 10 (2010) 4279 pMID: 20839780, http://dx.doi.org/10.1021/nl102931z.
[32] D. Song, G. Chen, Appl. Phys. Lett. 84 (2004) 687. http://scitation.aip.org/content/aip/journal/apl/84/5/10.1063/1.1642753.
[33] X. Xu, L.F.C. Pereira, Y. Wang, J. Wu, K. Zhang, X. Zhao, S. Bae, C. Tinh Bui, R. Xie, J.T.L. Thong, et al., Nat. Commun. 5 (2014b) 3689. ISSN 2041-1723, http://www.nature.com/doifinder/10.1038/ncomms4689.
[34] J. Bai, X. Duan, Y. Huang, Nano Lett. 9 (2009) 2083 pMID: 19344151, http://dx.doi.org/10.1021/nl900531n.
[35] L. Jiao, L. Zhang, X. Wang, G. Diankov, H. Dai, Nature 458 (2009) 877. ISSN 1476-4687, http://www.ncbi.nlm.nih.gov/pubmed/19370031.
[36] P.-H. Chang, M.S. Bahramy, N. Nagaosa, B.K. Nikolić, Nano Lett. 14 (2014) 3779. ISSN 1530-6992, http://www.ncbi.nlm.nih.gov/pubmed/24932511.
[37] P. Thiyagarajan, M.-W. Oh, J.-C. Yoon, J.-H. Jang, Appl. Phys. Lett. 105 (2014) 033905. ISSN 0003–6951, http://scitation.aip.org/content/aip/journal/apl/105/3/10.1063/1.4883892.
[38] J. Chen, G. Zhang, B. Li, Nano Lett. 10 (2010) 3978. ISSN 15306984, 1010.2861.
[39] T. Bauer, Int. J. Heat Mass Transf. 36 (1993) 4181.

[40] Y. Wang, B. Qiu, X. Ruan, Appl. Phys. Lett. 101 (2012) 013101. ISSN 00036951, http://link.aip.org/link/APPLAB/v101/i1/p013101/s1&Agg=doi.
[41] Y. Wang, C. Gu, X. Ruan, Appl. Phys. Lett. 106 (2015) 073104. ISSN 0003–6951, http://scitation.aip.org/content/aip/journal/apl/106/7/10.1063/1.4913319.
[42] G. Barbarino, C. Melis, L. Colombo, Carbon 80 (2014) 167. ISSN 00086223, http://linkinghub.elsevier.com/retrieve/pii/S0008622314007921.
[43] T. Feng, X. Ruan, J. Nanomater. 2014 (2014) 206370. ISSN 1687-4110, http://www.hindawi.com/journals/jnm/2014/206370/.
[44] S. Chen, Q. Wu, C. Mishra, J. Kang, H. Zhang, K. Cho, W. Cai, A. a. Balandin, R.S. Ruoff, Nat. Mater. 11 (2012) 203. ISSN 1476-1122, http://www.ncbi.nlm.nih.gov/pubmed/22231598.
[45] L. Lindsay, D.A. Broido, N. Mingo, Phys. Rev. B 82 (2010) 115427. ISSN 1098-0121, http://link.aps.org/doi/10.1103/PhysRevB.82.115427.
[46] L. Lindsay, D.A. Broido, Phys. Rev. B 84 (2011) 155421. ISSN 1098-0121, http://link.aps.org/doi/10.1103/PhysRevB.84.155421.
[47] J. Hu, S. Schiffli, A. Vallabhaneni, X. Ruan, Y.P. Chen, Appl. Phys. Lett. 97 (2010) 133107. ISSN 00036951, http://scitation.aip.org/content/aip/journal/apl/97/13/10.1063/1.3491267.
[48] D.W. Brenner, Phys. Rev. B 42 (1990) 9458. http://link.aps.org/doi/10.1103/PhysRevB.42.9458.